Hydration structures of the squarate dianion C 4O 4 2−. A combined molecular dynamics simulation and quantum ab initio study

ARTICLE *in* JOURNAL OF MOLECULAR STRUCTURE THEOCHEM · MARCH 2002

Impact Factor: 1.37 · DOI: 10.1016/S0166-1280(01)00608-X

3 AUTHORS, INCLUDING:

Pedro A. M. Vazquez
University of Campinas
33 PUBLICATIONS **133** CITATIONS
SEE PROFILE

Munir S Skaf
University of Campinas
85 PUBLICATIONS **1,733** CITATIONS
SEE PROFILE

ELSEVIER

Journal of Molecular Structure (Theochem) 580 (2002) 137-145

THEO CHEM

www.elsevier.com/locate/theochem

Hydration structures of the squarate dianion $C_4O_4^{2-}$. A combined molecular dynamics simulation and quantum ab initio study

Lucimara R. Martins*, Pedro A.M. Vazquez, Munir S. Skaf

Instituto de Química, Universidade Estadual de Campinas, Cx. P. 6154, Campinas, SP 13083-970, Brazil

Received 4 September 2000; accepted 22 January 2001

Abstract

Molecular dynamics (MD) simulations are used to determine the structure of the first solvation shell around a single monocyclic oxocarbon dianion $C_4O_4^{2-}$ in aqueous solution. The simulations were carried out using a fixed-geometry model for the oxocarbon with excess partial charges equally distributed over the oxygen atoms and the well-known SPC/E model for water. Quantum ab initio calculations for an isolated oxocarbon at different levels of approximation indicate that the such a description of the squarate dianion should be fairly accurate for the study of solvation structures. Analysis of a complete set of solute–solvent site–site radial distribution functions and hydrogen (H)-bonding distributions obtained from the MD simulations, indicates a well-defined first solvation shell consisting of approximately 18 water molecules. About 12 of these molecules are tightly H-bonded to the oxocarbon (an average of 3 molecules per oxygen atom) forming a highly symmetric solute–solvent complex, while the remaining six water molecules are more loosely distributed above and below the oxocarbon plane. The structure of a cluster consisting of a dianion and 12 water molecules was then examined through ab initio calculations at the Hartree–Fock 6-31G(d,p) level. The optimized ab initio structure of the cluster is in excellent agreement with the MD results.

Keywords: Molecular dynamics; Ab Initio; Oxocarbons; Hydration structures

1. Introduction

Oxocarbons are organic compounds in which most or all carbon atoms are bound to carbonyl groups or their equivalents [1]. The monocyclic dianions, $C_nO_n^{2-}$ ($3 \leq n \leq 6$; see Fig. 1), and their protonated forms are the most important archetypes within the oxocarbon family [1,2]. Among these, the derivatives of the squarate acid ($H_2C_4O_4$) have found many applications [2], including the squaric acid diethyl ester as a coupling reagent in the synthesis of selective antitumoral agents [3], the squaric acid and the squarate dianion as templates for controlling the assembly of stable, highly organized two-and three-dimensional crystalline aggregates of interest to material sciences [4], and several squaraines compounds as electron acceptors for nonlinear optical materials [5] and photovoltaic devices [6] due to their photochemical and photoconductive properties [7,8].

From the theoretical point of view, the literature on oxocarbons has focused almost exclusively on their peculiar electronic structure and spectroscopic features [9–14] The aromaticity of the oxocarbon dianions, especially of the squarate, has been one of the most challenging problems [13] in this context since West first proposed many years ago that these

* Corresponding author. Tel.: +55-19-3788-3093; fax: +55-19-3788-3023.

E-mail address: lucimara@iqm.unicamp.br (L.R. Martins).

0166-1280/02/$ - see front matter
PII: S0166-1280(01)00608-X

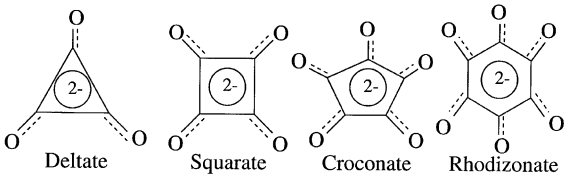

Fig. 1. Molecular structure of monocyclic oxocarbon dianions.

compounds form a class of nonbenzenoid aromatics [15]. Theoretical studies carried out recently by Schleyer et al. [13] and independently by Quiñonero et al. [14] on the aromaticity degree of oxocarbons found a NICS ('Nucleus-Independent Chemical Shift') of −8.6 for the squarate, which places this anion below benzene and the deltate dianion (NICS of −10.0 and −11.0, respectively), thus characterizing the squarate as moderately aromatic. The 5 and 6 membered rings are found to be much less aromatic. From the electronic structure standpoint, the squarate dianion emerges as one of the few examples where, due to the degeneracy of the first singlet state, the Raman active non-totally symmetric vibrational normal modes derive their intensities from the Jahn–Teller effect [16]. Very recently, it has been experimentally found that the excess charge on this anion leads to formation of ligand to metal charge transfer complexes confirming its effective ligand character [17].

Despite the rapidly increasing number and diversity of applications of these compounds in recent years and the body of theoretical work devoted to their electronic structure properties, the behavior of oxocarbon dianions in solution remains largely unexplored. In particular, the strong hydrogen(H)-bond acceptor character of the oxocarbon dianions [2] combined with their distinctive planar shape [18] suggest on the outset that these compounds may exhibit interesting solvation properties in aqueous and other protic environments. Although no specific investigation of the structure of solutions containing oxocarbon dianions (e.g. via X-ray, electron or neutron diffraction experiments) have been reported so far, X-ray diffraction of monohydrated $K_2C_4O_4$ and $LiHC_4O_4$ crystals shows evidence of H-bonding between the dianion and water [19,20]. In a recent study, Ribeiro et al. [21] observed that the Raman bandshapes of both totally symmetric and non-totally symmetric modes of the squarate and croconate ($n = 5$) dianions in water strongly suggest the existence of structurally well-defined solvent cages, such as those formed through H-bonding with the solute.

In this work, we report for the first time a detailed theoretical analysis of the hydration structure of a single $C_4O_4^{2-}$ dianion in solution using molecular dynamics (MD) simulations methods. Our primary goal here is to examine the formation of solute–solvent H-bonding at ambient conditions and to provide a first view of the solvent structure in the immediate vicinity of the solute. Dynamical properties of this system shall be addressed in a forthcoming work. A quantum ab initio survey at the Hartree–Fock and Density Functional Theory (DFT) levels for the anion alone and at the Hartree–Fock 6-31G(d,p) level for clusters containing the anion plus several water molecules were also performed in order to gain qualitative insights into the conformational stiffness of the squarate and stability of the hydration structure, thus assessing the performance of the simulation force-field in describing the solvation structure. These aspects are particularly important here given the absence of experimental measurements on the structure of these aqueous solutions that could be used to gauge the accuracy of the MD results.

In the next section, we describe the computational details of the simulation, the force-field parameters, and the ab initio calculations. Our main results and discussion are presented in Section 3. The concluding remarks are finally presented in Section 4..

2. Computational details

2.1. Interaction potentials and MD simulations

In the simulations, the squarate dianion $C_4O_4^{2-}$ is described by a rigid, planar molecular geometry of D_{4h} symmetry [18] in which the C–C and C–O bondlengths are 1.47 and 1.26 Å, respectively [19]. The CCC and OCC angles are 90 and 135° (see Fig. 1). For water, we have used the well-known three-site SPC/E (extended simple point charge) model [22], which describes well the thermodynamics, structure and dynamical properties of neat water and solutions. For the SPC/E model, the O–H distance is 1.0 Å and the HOH angle is 104.5°. The potential energy for both

Table 1
Interaction potential parameters for SPC/E water and the squarate dianion

Site	σ (Å)	ϵ/k_B (K)	Charge (e)
O_w	3.17	78.48	−0.8476
H	0.00	0.000	0.4238
O_{oxo}	2.96	105.68	−0.851
C	3.75	52.84	0.351

solute and solvent molecules are prescribed by pair additive interaction-site potentials consisting of Lennard–Jones plus Coulombic terms centered on each atom:

$$V_{ij}(r) = 4\epsilon_{ij}\left[\left(\frac{\sigma_{ij}}{r}\right)^{12} - \left(\frac{\sigma_{ij}}{r}\right)^{6}\right] + \frac{q_i q_j}{4\pi\epsilon_0 r}, \qquad (1)$$

where q_i is the partial charge on site i, ϵ_{ij} and σ_{ij} are the Lennard–Jones parameters, and r is the distance between sites i and j on different molecules. For sites of different types we used the usual Lorentz–Berthelot [23] combination rules, $\epsilon_{ij} = (\epsilon_{ii}\epsilon_{jj})^{1/2}$ and $\sigma_{ij} = (\sigma_{ii} + \sigma_{jj})/2$. Lennard–Jones parameters for the atoms on the oxocarbon were taken from the OPLS (optimized potential for liquid simulations) force-field [24] for similar ligands without further refinements. This is justified here in view of the lack of available experimental data which could be used as targets in a parametrization procedure for the oxocarbon in solution. The set of Mulliken partial charges on the oxocarbon used here were obtained from the ab initio calculations of Puebla and Ha [10]. These charges are in close agreement with those obtained recently by Schleyer et al. [13] and also with our own quantum calculations, as shown below. Additional details of the interaction potentials are found in Table 1, where the oxygens atoms for water and oxocarbon are denoted O_w and O_{oxo}, respectively.

The simulations were performed in the NVE ensemble for solutions containing a single $C_4O_4^{2-}$ anion and $N = 499$ water molecules placed in a cubic box whose dimensions are such as to match the solvent density at ambient conditions ($\rho = 0.033$ molecules/Å^3). The resulting average pressure was nearly 1 bar at an average temperature of 298 K. We applied minimum image convention with a cut-off at half the box length for the Lennard–Jones forces. The long-range Coulombic forces were treated via Ewald sums with conducting boundaries [23]. The equations of motion were integrated using the leaf-frog and quaternions algorithms [23] with a timestep of 1 fs. This enabled total energy conservation within 0.1% error during uninterrupted runs of 10 ps. Between 125 and 150 equilibrated runs of 10 ps were used for data analysis, each separated by smaller runs (3 ps) during which the velocities were rescaled to yield the desired temperature (298 K). The trajectories were discarded during velocity rescaling.

2.2. Ab initio calculations

Two separate systems were considered for the ab initio analysis. For the conformation and partial charges of the squarate anion alone, we performed Hartree–Fock 6-31G(d,p) and DFT B3LYP 6-31++G** calculations using the GAUSSIAN94 suite [25]. For the oxocarbon plus 12 water molecules cluster, the calculations were done at the Hartree–Fock level. The 6-31G basis set was used with polarization functions at all carbons and oxygens atoms, additional diffuse functions were added only to the oxocarbon oxygen atoms. The clusters were formed by coordinating 12 water molecules around the oxocarbon dianion according to the structural data obtained from the simulations. The resulting complex was optimized maintaining the planar structure of the dianion fixed and also in the absence of such a constraint.

3. Results and discussion

3.1. Molecular dynamics analysis

We start our discussion by investigating the formation of H-bonding between water molecules and the squarate dianion through its O_{oxo} atoms. A well-established geometric criterion suitable for molecular simulations [26] is used to determine the existence of an H-bonding between solute–solvent pairs. Namely, two molecules are H-bonded when the following three conditions are simultaneously satisfied: (i) The distance $O_\alpha\cdots H$ should be no greater than 2.6 Å; (ii) The distance $O_\alpha\cdots O_w$ should be smaller than 3.5 Å; and (iii) The angle $O_\alpha O_w H$ should not

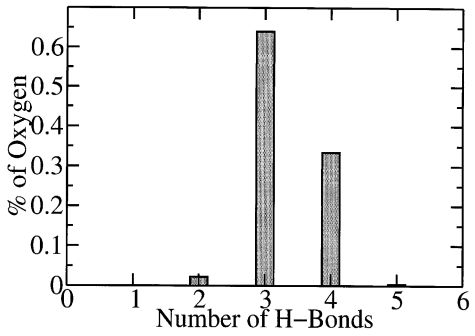

Fig. 2. MD results for the distribution of solute–water hydrogen bonding per oxocarbon oxygen atom.

exceed 30°. This H-bond definition is equally applicable to oxocarbon–water (i.e. α = oxo) and water–water (i.e. α = w) pairs since the Lennard–Jones diameters for O_{oxo} and O_w are similar to each other. The resulting distributions of oxocarbon–water H-bonds calculated from the MD trajectories are depicted in Fig. 2, where the horizontal axis indicates the number of H-bonds formed per O_{oxo} atom. The distribution is sharply peaked (64%) at three water molecules per oxygen atom on the squarate ion, but there is a considerable occurrence (33%) of four water molecules bonded to a given O_{oxo} atom. The relative occurrence of one and five H-bonds per solute acceptor center is negligible. The average O_{oxo}–O_w and O_{oxo}–H distances for bonded pairs are respectively, 2.6 and 1.6 Å.

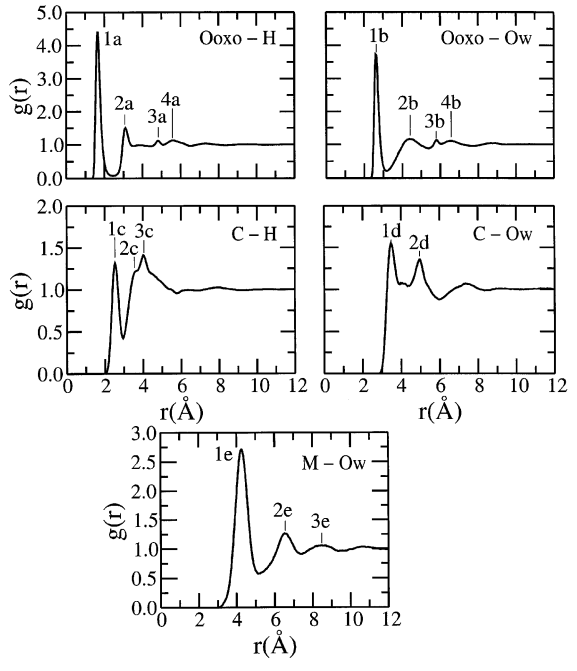

Fig. 3. Solute–water site–site radial distribution functions obtained from the MD simulations.

The H-bond distribution for water–water pairs has also been calculated for different regions within the solution in order to examine how the oxocarbon affects the structure of the surrounding solvent. We find that a water molecule located within the first hydration shell (i.e. within 4.2 Å from the anion center. See below) is H-bonded to 3 other water molecules, whereas in the bulk, water typically forms an average of 4 H-bonds per molecule. This simply reflects the fact that molecules nearest to the solute engage in an H-bond to the oxocarbon oxygen, thus shifting the distribution one unit down. Beyond the first shell, the distribution of H-bonds turns out very similar to the pure liquids, suggesting that despite the size and shape of the solute, its presence does not lead to drastic disruption of water's ubiquitous H-bonding pattern.

The overall picture of the solvent organization around the oxocarbon dianion can be conveniently examined through an analysis of the radial distribution functions (RDFs), $g_{ij}(r)$, between the oxocarbon and water sites. The results for all distinct solute–solvent site–site pairs are displayed in Fig. 3, along with the RDF for the pair of solute center of mass (M_{oxo}) and water oxygen. Panels a–e depict the RDFs for the $O_{oxo}H$, $O_{oxo}O_w$, CH, CO_w, and $M_{oxo}O_w$ pairs, respectively. First and second solvation shells are defined by the first and second minima of the $M_{oxo}O_w$ RDF, located at 4.2 and 7.2 Å, respectively. Integration of $4\pi\rho r^2 g(r)$ for this pair of sites up to 4.2 Å yields an average of 18.3 water molecules in the first coordination shell. Similarly, the first peaks of the corresponding RDFs yield approximately 3.1 hydrogens and 3.2 water oxygens coordinating each O_{oxo} atom, in accord with the H-bond distribution discussed above. Indeed, the first peaks of the $O_{oxo}O_w$ and $O_{oxo}H$ RDFs are very characteristic of H-bonding. Their positions are ~1.0 Å apart from each other, indicating that the H-bond $O_{oxo}\cdots HO_w$ is on the

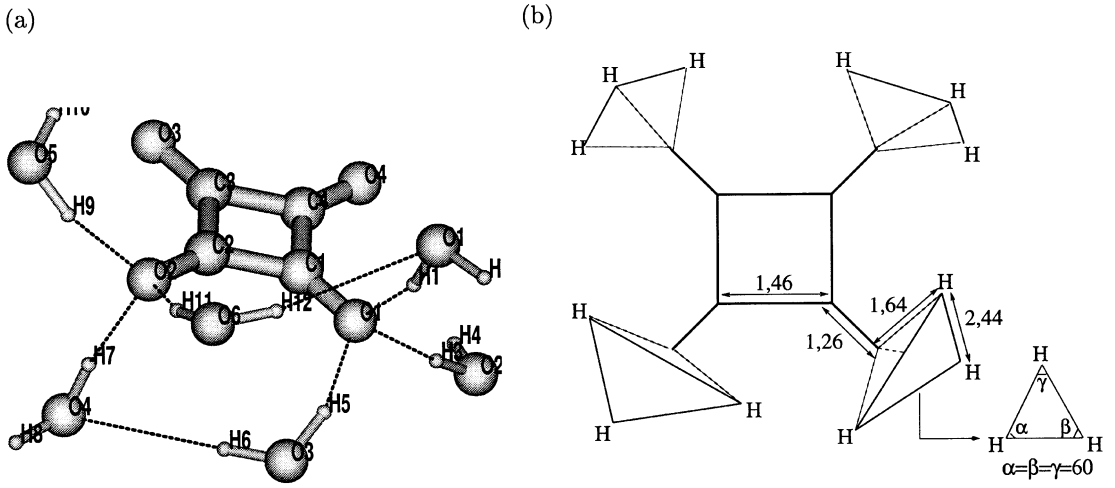

Fig. 4. Schematic representation of the structure of the first hydration shell obtained from the MD simulations. The first hydration shell consists of 18 molecules, 12 of which are H-bonded to the solute, while the other 6 (not shown) are distributed above and below the oxocarbon plane.

average linear [27]. [1] Moreover, these results indicate that only ~12 out of the 18 water molecules comprising the first hydration shell are H-bonded to the dianion.

One of the most conspicuous features in these RDFs, is the existence of sharply defined structures appearing in the $O_{oxo}H$ and $O_{oxo}O_w$ curves extending over separations as large as 5 or 7 Å (cf. the peaks marked 2b–4b in Fig. 3b). The presence of such structures in the RDFs signifies a considerable degree of correlations between the oxocarbon oxygens and the surrounding water molecules. At first, one could naively speculate that these features stem from outer solvation shells. However, the prominent first peaks of the RDFs around the O_{oxo} atoms and the symmetrical shape of the oxocarbon dianion suggest that these short, but well-resolved peaks may reflect solute–solvent pairs consisting of water molecules tightly first-coordinated to an oxygen atom of the solute and the remaining three O_{oxo} atoms. Using Molden, a molecular graphics package [28], and elementary analytical geometry applied to the set of data of Fig. 3, we have been able to show that this is indeed the case. The average structure of first hydration shell of the squarate dianion so obtained, turns out highly symmetrical, where water molecules may simultaneously H-bond to the solute and to other solvent molecules within the first shell, as shown in Fig. 4.

The average structure of the first hydration shell is portrayed in Fig. 4a, where only six of the approximately 18 water molecules are shown. The three hydrogen atoms (of distinct water molecules) H-bonded to an O_{oxo} atom form an equilateral triangle lying perpendicularly to the oxocarbon plane. Adjacent triangles have vertices pointing in opposite directions, as schematically shown in Fig. 4b, totaling 12 solvent molecules H-bonded to the solute. The remaining 6 water molecules (not H-bonded to the solute) are scattered above and below the oxocarbon plane. An inspection of the molecular trajectories along the entire course of the simulation, reveals that these molecules interchange frequently between first, second, and outer solvation shells, whereas the 12 molecules that are H-bonded to the solute remain in the first hydration shell for considerably long periods of time (≈ 15–25 ps). The H-bonds between a pair of water molecules surrounding distinct carbonyl groups (e.g. the bond $H12\cdots O_w1$) are not as long lived as the solute–solvent H-bonds. The hydrogen atoms that are not bonded to the solute (for instance, H12) may rotate during the course of the simulation due to thermal fluctuations, leading to a continuous breaking and forming of these water–water H-bonds. The

[1] Although individual H-bonds are seldom linear, such an average geometry is frequently found for other H-bond acceptor solutes in water.

Table 2
Assignements of selected peaks in the radial distribution functions of Fig. 3 for the oxocarbon-12 water complex. The atoms are labeled according to Fig. 4a

Peak label	Position (Å)	Site pair
1a	1.6	$O_{oxo}1$ H1, $O_{oxo}1$ H3, $O_{oxo}1$ H5
2a	3.1	$O_{oxo}1$ H2, $O_{oxo}1$ H4, $O_{oxo}1$ H6, $O_{oxo}1$ H12
3a	4.8	$O_{oxo}1$ H9
4a	5.6	$O_{oxo}1$ H8, $O_{oxo}1$ H10
1b	2.6	$O_{oxo}1$ O_w1, $O_{oxo}1$ O_w2, $O_{oxo}1$ O_w3
2b	4.4	$O_{oxo}1$ O_w4, $O_{oxo}1$ O_w6
3b	5.8	$O_{oxo}1$ O_w5
1c	2.5	C1 H1, C1 H3, C1 H5
2c	3.6	C1 H2, C1 H4, C1 H6, C1 H11, C1 H12
3c	4.0	C1 H7, C1 H9
1d	3.5	C1 O_w1, C1 O_w2, C1 O_w3, C1 O_w6
2d	5.0	C1 O_w5

estimated lifetime is only somewhat larger than the H-bond lifetime in bulk water (~1 ps) [26]. The peaks labeled 1a–4b in Fig. 3 can be assigned to specific average site–site distances in the drawing shown in Fig. 4a, as summarized in Table 2. Peaks 1a–d stem from the pairs $O_{oxo}1$ H1 and their equivalents, peaks 3a–c stems from the correlations between one carbonyl group with the solvent molecules surrounding an adjacent carbonyl (e.g. $O_{oxo}1$ H9, $O_{oxo}1$ O_w5, C1 H9), and so forth.

3.2. Ab initio results

In this work all MD simulations were carried out within a classical model where the squarate anion is described by a rigid framework with classic point charges derived from quantum molecular orbital calculations using the Mulliken charge model [10]. Aiming to evaluate the limitations and adequacy of this model, a series of quantum calculations were carried out on the squarate anion and are now described.

Table 3
Atomic charges on the dianion $C_4O_4^{2-}$ obtained from the Hartree–Fock 6-31G(d,p) calculations

Site	Mulliken	CHELP	CHELPG	Bader
C	0.3841	0.3846	0.3321	0.9852
O	−0.8841	−0.8846	−0.8321	−1.4880

First, the charges used on the MD simulation were compared with those derived by the AIM (atoms in molecules theory) [29] and CHELPG (charges from electrostatic potentials-grid based) [30,31] calculated with GAUSSIAN94 at the Hartree–Fock and DFT levels for a single dianion. The results show that the CHELPG method yields charges slightly smaller than those used by us (Mulliken; see also Table 3), whereas the AIM charges are considerably higher. Given the success and popularity of CHELPG charges for MD applications [30], these results indicate that the charges used in the present simulations seems quite appropriate. In addition, we have also performed an analysis of the natural orbital occupations derived from MP2 calculations with the 6-31++G** basis in order to examine to what extent the Hartree–Fock orbital occupation is adequate for this anion. The analysis shows that this anion has an excess charge spread over the molecular orbitals with an occupation of 57.2 electrons below the HOMO, while the HOMO itself is occupied with 1.9 electrons, validating the Hartree–Fock approximation (2 electrons per orbital) for the present purposes. The excess charge observed on the natural orbital analysis suggests a tendency of this molecule to structure solvent molecules around the charge excess centers, that is, the oxygen atoms. This is nicely borne out by the MD results presented above. On the other hand, the localization of excess charge towards the oxygen centers also implies a depletion of resonant π-electrons over the backbone and an eventual diminution of the backbone stiffness, which is partially compensated through the electrostatic repulsion between the negative charge centers [32].

Moreover, the internal vibrational frequencies of the squarate were determined at the Hartree–Fock 6-31(d,p) and DFT B3LYP 6-31++G** levels. The results, displayed in Table 4, are seen to agree very well with earlier [18] as well as more recent infrared and Raman experimental measurements [17,21]. Our calculations indicate the presence of low-frequency modes associated with an out-of-plane motions of the oxygen atoms below 100 cm^{-1} (namely, 70 and 99 cm^{-1} at the HF and DFT levels, respectively). These modes are predicted below the frequency

Table 4
Vibrational frequencies in cm^{-1} for the squarate dianion calculated in this work at the HF and DFT levels, and the corresponding experimental data. The normal mode attibutions and symmetry assignments are found in Ref. [1]

Attribution	Ito e West [18]		Ab initio	DFT	Ribeiro [21]	Gonçalves [17]	
	IV	Raman	6-31G(d,p)	B3LYP/6-31++G**		Solid	Liquid
–	–	–	70	99	–	–	–
$\nu_4 - A_{2u}$	259	–	292	254	–	259	–
$\nu_6 - B_{1g}$	–	294	285	284	–	321	301
$\nu_{14} - E_u$	350	–	329	333	–	350	–
$\nu_{10} - B_{2g}$	–	647	650	648	644	650	647
–	–	–	520	676	–		
$\nu_{11} - E_g$	–	662	633	676	–	662	663
$\nu_2 - A_{1g}$	–	723	724	723	722	726	724
$\nu_3 - A_{2g}$	–	–	866	872	–		
$\nu_{13} - E_u$	1090	–	1114	1113	–	1087	1090
$\nu_5 - B_{1g}$	–	1123	1227	1113	1121	1131	1123
$\nu_2 + \nu_{11}$	–	1329	–	–	–	1319	
$\nu_{12} - E_u$	1530	–	1513	1593	–	1530	–
$\nu_9 - B_{2g}$	–	1593	1686	1680	–	1607	1591
$\nu_1 - A_{1g}$	–	1794	1866	1847	–	1797	1791
$\nu_5 + \nu_{13}$	2200	–	–	–			

range of the available experimental data, which prevents direct comparison with spectroscopic measurements at this point. Similar modes have also been theoretically obtained by Cerioni et al. [32]. The fact that energy of these modes is less than half the thermal energy at 298 K ($207\ cm^{-1}$) suggests that backbone torsions are likely to be coupled to the motions of the solvent bath. The effects of such coupling upon the spectroscopic properties of the dianion in solution warrant further investigation. More importantly within the context of the present work, however, is whether eventual distortions from the average planar geometry of the solute have any significant impact on the hydration structure.

Before proceeding in that direction, let us consider the energies involved in distorting the planar backbone of the squarate. The torsional energy, defined as the energy difference between the distorted and planar molecules as a function of the C–C–C–C dihedral angle, has been calculated at both levels of theory and are depicted in Fig. 5. The dihedral angle was kept fixed at 1° intervals from 0 to 10° while the other internal coordinates were optimized. The results show a modest 10 cal/mol cost for angular displacements of the order of 1°. However, there is a marked increase in the energy cost with the torsion angle. For torsions of about 10° or so, the torsional energy is at least of the order of the thermal energy (~0.6 kcal/mol). Therefore, mild conformational distortions about the plane should not be ruled out in the presence of the solvent. The quantitative differences between the HF and DFT energy barriers reflect the electron correlation effects present in the DFT calculation. The interesting observation is that the physical features emerging from both calculations follow similar trends irrespective of the level of the approximations used.

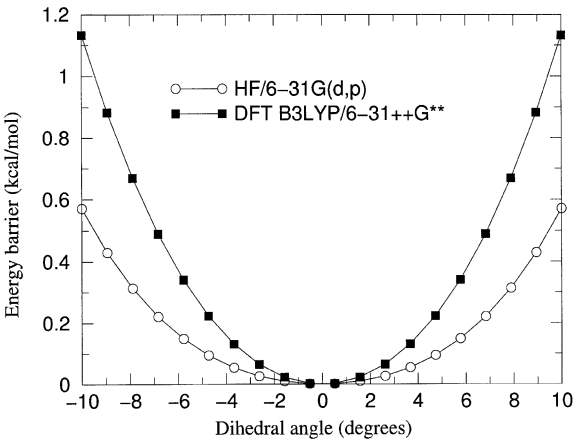

Fig. 5. Torsional energy barriers for the squarate dianion as functions of the C–C–C–C dihedral angle calculated at the Hartree–Fock (empty circles) and DFT (filled squares) levels.

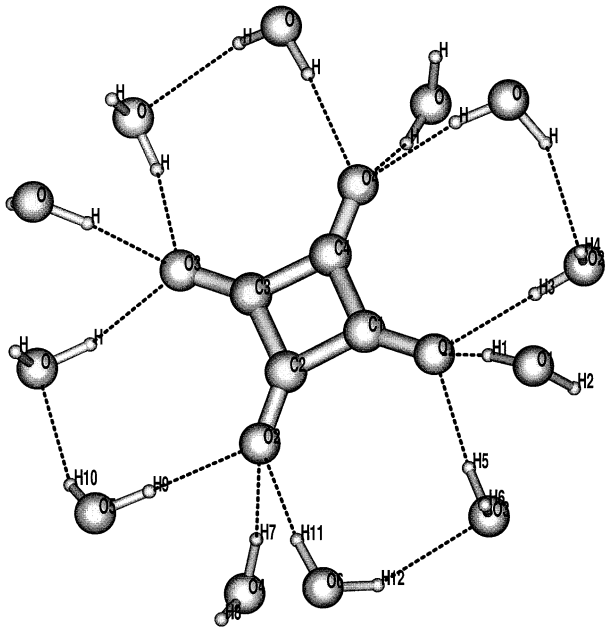

Fig. 6. Optimized structure for a cluster consisting of planar squarate dianion plus 12 water molecules as obtained from ab initio Hartree–Fock calculation using the 6-31G(d,p) basis set.

To conclude our analysis, we discuss the quantum ab initio results performed at the Hartree–Fock 6-31G(d,p) level for clusters comprising of the anion plus 12 water molecules. The calculations were performed using the structure predicted by the MD simulations or small variants thereof as starting points. Separate calculations were performed keeping the geometry of the anion fixed on a plane and also in the absence of such constraint. In both cases, the optimized structures portray patterns of solute–solvent H-bonds and corresponding interatomic separations very similar to those found via MD. The optimized structure for the cluster with a planar anion is depicted in Fig. 6. There are three water molecules H-bonded to each O_{oxo} atom. The interatomic separations are given in Table 5 along with the average values determined from the simulations, showing very good agreement. The H-bonding between neighboring water molecules within the cluster turned out somewhat distinct from that found in the simulations. For instance, in the ab initio optimized structure an H-bond is formed between H12 and O_w3, whereas in the MD, H12 is expected to be bonded to O_w1. This aspect, however, is of secondary importance since water–water hydrogen bonds continuously break and re-form due to thermal fluctuations, as noted above. When the geometrical constraint on the anion is lifted, its conformation in the presence of the solvent is stabilized by a small torsion of the plane, with the C–C–C–C dihedral angle being not larger than ~8°. The torsion of the ring is such that adjacent O_{oxo} atoms are pulled in opposite directions with respect to the anion 'plane'. This effect can be qualitative accounted for by the alternating effective attractions of the H-bonds to the solvent molecules, as can be seen in Figs. 4 and 6.

Table 5
Average solute–solvent nearest neighbor distances from MD and ab initio calculations

Sites	Average distance (Å) MD	Average distance (Å) ab initio
O_{oxo}–O_w	2.6	2.7
C–H	2.5	2.6
O_{oxo}–H	1.64	1.79
C–O_w	3.4	3.5

4. Concluding remarks

We have presented a detailed study of the structural properties of the hydration shell around the oxocarbon dianion $C_4O_4^{2-}$ based on MD simulations and quantum ab initio calculations. We find a highly symmetric and stable solvent cage around the anion, consisting of 12 water molecules H-bonded to the oxocarbon oxygen (3 water molecules per O_{oxo}). The hydration structure is completed with 6 additional water molecules distributed above and below the dianion plane. These molecules are continuously exchanged with the bulk. The ab initio calculations for clusters containing the anion and 12 water molecules yield optimized structures very similar to the ones predicted by MD. In addition, the ab initio natural orbital population analysis and conformational properties of the anion provides support to the adequacy of the oxocarbon model employed in the simulations.

Work is currently underway aiming at exploring the dynamical and spectroscopic behavior of oxocarbons in aqueous solutions. In particular, we hope to examine the rotational–translational diffusion as well as the fast reorientational motions of these ions in solution in the light of the hydration structures presented here. We hope to correlate structural and dynamical features of these solutions in order to investigate available Raman spectroscopy data [21] from a more detailed, microscopic perspective.

Acknowledgements

The financial support provided by the Brazilian agencies FAPESP (99/09879-6 and 97/13535-5) and CNPq is gratefully acknowledged.

References

[1] R. West (Ed.), Oxocarbons Academic Press, New York, 1980.
[2] G. Seltz, P. Imming, Chem. Rev. 92 (1992) 1227.
[3] L.F. Tietze, C. Schroder, S. Gabius, U. Brinck, A. Goerlach-Graw, H.-J. Gabius, Bioconjugate Chem. 2 (1991) 148.
[4] I.L. Karle, D. Ranganathan, V. Haridas, J. Am. Chem. Soc. 118 (1996) 7128.
[5] L.S. Pu, J. Chem. Soc., Chem. Commun. 6 (1991) 429.
[6] Y. Kobayashi, M. Goto, M. Kurahashi, Bull. Chem. Soc. Jpn. 59 (1986) 311.
[7] B. Zhao, M.H. Back, Can. J. Chem. 69 (1991) 528.
[8] V.Y. Merrit, H.J. Hovel, Appl. Phys. Lett. 29 (1978) 414.
[9] J. Aihara, J. Am. Chem. Soc. 103 (1981) 1633.
[10] C. Puebla, T.-K. Ha, J. Mol. Struct. (Theochem) 137 (1986) 171.
[11] W.C. Herndon, J. Mol. Struct. (Theochem) 103 (1983) 219.
[12] L. Zhou, Y. Zhang, L. Wu, J. Li, J. Mol. Struct. (Theochem) 497 (2000) 137.
[13] P.R. Schleyer, K. Najafian, B. Kiran, H. Jiao, J. Org. Chem. 65 (2000) 426.
[14] D. Quiñonero, A. Frontera, P. Ballester, P.M. Deyà, Tetrahedron Lett. 41 (2000) 2001.
[15] R. West, N.-Y. Niu, D.L. Powell, M.V. Evans, J. Am. Chem. Soc. 826 (1960) 204.
[16] M. Takahasi, K. Kaya, M. Ito, Chem. Phys. 35 (1978) 293.
[17] P.S. Santos, O. Sala, L.K. Noda, N.S. Gonçalves, Spectrochim. Acta A 56 (2000) 1553.
[18] M. Ito, R. West, J. Am. Chem. Soc. 85 (1963) 2580.
[19] W.M. MacIntyre, M.S. Wekerma, J. Chem. Phys. 40 (1964) 3563.
[20] D. Semmingsen, Acta Chem. Scand. 30 (1976) 808.
[21] M.C.C. Ribeiro, L.F.C. de Oliveira, P.S. Santos, Chem. Phys. 217 (1997) 71.
[22] H.J.C. Berendsen, J.R. Grigera, T.P. Straatsma, J. Phys. Chem. 91 (1987) 6269.
[23] M.P. Allen, D.J. Tildesley, Computer Simulations of Liquids, Oxford University Press, Clarendon Park, 1987.
[24] W.L. Jorgensen, D.L. Severence, J. Am. Chem. Soc. 112 (1990) 4768.
[25] M.J. Frisch, G.W. Trucks, H.B. Schlegel, P.M.W. Gill, B.G. Johnson, M.A. Robb, J.R. Cheeseman, T. Keith, G.A. Petersson, J.A. Montgomery, K. Raghavachari, M.A. Al-Laham, V.G. Zakrzewski, J.V. Ortiz, J.B. Foresman, J. Cioslowski, B.B. Stefanov, A. Nanayakkara, M. Challacombe, C.Y. Peng, P.Y. Ayala, W. Chen, M.W. Wong, J.L. Andres, E.S. Replogle, R. Gomperts, R.L. Martin, D.J. Fox, J.S. Binkley, D.J. Defrees, J. Baker, J.P. Stewart, M. Head-Gordon, C. Gonzalez, J.A. Pople, GAUSSIAN94, Revision D.2. Gaussian, Inc., Pittsburgh, PA, 1995.
[26] B.M. Ladanyi, M.S. Skaf, Annu. Rev. Phys. Chem. 44 (1993) 335.
[27] H. Ohtaki, T. Radnai, Chem. Rev 93 (1993) 1157.
[28] G. Schaftenaar, J.H. Noordik, J. Comp.-Aided Mol. Des. 14 (2000) 123.
[29] R.F.W. Bader, Atoms in Molecules: A Quantum Theory, Oxford University Press, Oxford, 1990.
[30] U.C. Singh, P.A. Kollman, J. Comp. Chem. 5 (1984) 129.
[31] C.M. Breneman, K.B. Wiberg, J. Comp. Chem. 11 (1990) 361.
[32] G. Cerioni, R. Janoschek, Z. Rappoport, T.T. Tidwell, J. Org. Chem. 61 (1996) 6212.